Calculation of Steel Stresses in Cracked Reinforced Rectangular Concrete Elements Loaded in Bending

I. Anton van der Esch(✉), Rob Wolfs, and Simon Wijte

Eindhoven University of Technology, 5612 AZ Eindhoven, The Netherlands
i.a.v.d.esch@tue.nl

Abstract. An accurate calculation of steel stresses is essential for assessing reinforced concrete structures' serviceability limit state, e.g., assessing crack widths. The steel stresses in elements loaded in bending are not known but are estimated by steel stress calculations. To get a more accurate crack width prediction, the calculated steel stress should approximately represent the actual steel stress at the location of the crack after the crack has been formed. Existing methods for calculating steel stresses are frequently based on numerous assumptions; e.g., the tensile stresses or tension softening effects in the cross-section are neglected, and a linear stress-strain distribution is assumed for the concrete in compression. This paper presents a method to calculate steel stresses based on existing constitutive theoretical relations that consider concrete's non-linear behaviour in compression and tension. They are compared with strain measurements of the reinforcement bars using distributed optical fiber sensors obtained from experiments described in the literature. Results showed that existing methods frequently overestimated the steel stress, especially when the first cracks were formed. Therefore, a method was developed for an improved calculation of steel stresses in elements loaded in bending with a rectangular cross-section. The paper demonstrated that the developed method could estimate steel stresses more accurately from the first to the final crack. The presented method applies to rectangular cross-sections with a single reinforcement layer but can be straightforwardly extended to other shapes in a similar procedure and can be used to assess the accuracy of crack width formulations based on experimental results.

Keywords: cracking · bending · steel stresses · tension softening

1 Introduction

An accurate description of crack widths w is essential to check if crack width limits w_{lim} for ingress rates are met [1–3]. The values of w can be calculated by crack width formulations, e.g., as described in EN1992–1-1 [4]. In these formulations, an important parameter is the steel stress σ_s, at the location of the considered crack [5]. σ_s can readily be obtained for elements subjected to a pure tension force with symmetric reinforcement since the strain over the height h of the cross section is uniform, leading to an equal

© The Author(s), under exclusive license to Springer Nature Switzerland AG 2023
A. Jędrzejewska et al. (Eds.): SynerCrete 2023, RILEM Bookseries 43, pp. 1047–1058, 2023.
https://doi.org/10.1007/978-3-031-33211-1_94

force distribution in the reinforcement. However, obtaining an accurate value for σ_s for elements loaded in bending, is more complex than for the pure tension case, since the non-linear behavior at the compressive side of the element and the tension softening part of the cracked section partly determine the internal force distribution in the concrete [6]. Therefore, numerous methods were developed based on simplifications to estimate σ_s at the location of a crack, denoted as $\hat{\sigma}_s$ [7–9]. The methods frequently assume a linear-elastic behaviour of concrete in compression and neglect the contribution of concrete in tension [10], leading to an overestimation of σ_s, especially for the stage when the first cracks in the element are developing. This can lead to an overestimation of crack widths, which results in a higher reinforcement ratio ρ, thus increasing costs. Moreover, a comparison between various crack width formulations shows that the influence of $\hat{\sigma}_s$ on the crack width varies [5, 11]. To conclude, a workflow and method are needed to accurately estimate these steel stresses in reinforced concrete elements loaded in bending.

The goal of this paper is to develop a method to calculate σ_s for the entire cracking process for elements loaded in bending. First, a short literature review discusses various methods for calculating σ_s. Then, a new semi-analytical approach is presented, including concrete's non-linear compression and tension softening behaviour, based on existing constitutive relations. Afterwards, the model is validated based on existing experiments using distributed optical fiber sensors (DOFs). Finally, the paper discusses how the results can be used for further research and how they can be improved.

2 Methods for Calculating σ_s in Elements Loaded in Bending

2.1 Assuming a Triangular Compression Zone

Frequently, $\hat{\sigma}_s$ is calculated based on equilibrium equations. The concrete compression zone x_c, in the case of a rectangular cross-section with a single layer of reinforcement, is often derived analytically, based on horizontal equilibrium and under the assumption of a triangular shape of the compression zone [7]. The triangular shape follows from the assumption that plane sections remain plane, and a linear stress-strain relation is adopted for concrete in compression. The formula for x_c based on these assumptions is given by

$$x_c = d\left(-\alpha_e\rho + \sqrt{(\alpha_e\rho)^2 + 2\alpha_e\rho}\right), \tag{1}$$

where d is the working height, ρ the longitudinal reinforcement ratio and $\alpha_e = E_s/E_c$, where E_s denotes the modulus of elasticity of the reinforcement steel. In this paper, the short-term modulus of elasticity of concrete E_c is used since it coincides with adopted constitutive relations later in this paper that also make use of the short-term E_c. $\hat{\sigma}_s$, at the location of a crack, can be calculated as

$$\hat{\sigma}_s = \frac{1}{A_s}\frac{M_{ext}}{d - \frac{x_c}{3}}, \tag{2}$$

where M_{ext} denotes the applied bending moment and A_s the reinforcement area. Equations (1) and (2) are based on the assumptions of a rectangular cross-section, the presence of pure bending, the neglection of tensile stresses in the concrete below the neutral axis, and an evenly distributed tensile force over the various reinforcement bars, having a single layer of reinforcement. Van der Schrier [7] derived Eqs. (1) and (2); therefore, in this paper, the method based on these equations is called the Schrier method.

2.2 Assuming Linear Interpolation Between M_{ext} and M_R

Another frequently used method is to estimate σ_s based on the ratio of the bending moment M_{ext} in the SLS, and the ultimate bending moment capacity M_R. The latter is calculated as

$$M_R = A_s f_y \left(d - \frac{14}{27} \frac{A_s f_y}{f_{cm} b} \right) \tag{3}$$

and can be derived from horizontal and moment equilibrium. In Eq. (3), b denotes the width of the cross-section, f_{cm} the mean value of the compressive strength of the concrete and f_y the yield strength of the reinforcement. The factor 14/27 is based on the stress-strain relation for concrete classes up to C50/60 [4]. According to [8], $\hat{\sigma}_s$ can now be calculated as

$$\hat{\sigma}_s = f_y M_{ext} / M_R. \tag{4}$$

This method is based on the same assumptions as the Schrier method, except that the height of x_c is based on an interpolation of M_{ext}/M_R. Equations (3) and (4) will be called the Interpolation method in this paper.

3 Development of the New Semi-analytical Method

Like the previously presented methods, the derivation of the semi-analytical method started with the analytical derivation of the horizontal and bending moment equilibrium equations. For the assumed directions in the equilibrium, see Fig. 1. The resulting equations for the horizontal force and bending moment are, respectively, given by

$$F_c - F_{t,1} - F_{t,2} - F_s = 0 \tag{5}$$

and

$$-M_{ext} + F_c \left(\frac{h}{2} - (x_c - z_c) \right) - F_{t,1} \left(\frac{h}{2} - x_c - \frac{2x_{t,1}}{3} \right) - F_{t,2} \left(\frac{h}{2} - x_c - x_{t,1} - z_{t,2} \right) + F_s \left(d - \frac{h}{2} \right) = 0, \tag{6}$$

where the reference point for the bending moments was taken on the horizontal symmetry line. The various parts of Eqs. (5) and (6) are depicted in Fig. 1 and are further explained and calculated in Eqs. (7)–(23).

A non-linear concrete compression stress-strain relation represents the concrete compression behaviour. The assumed relation was adopted from EN1992–1-1 [4] and *fib* Model Code 2010 [6] and is given by.

$$\sigma_c = f_{cm} \left(\frac{\eta(k - \eta)}{1 + \eta(k - 2)} \right) for\ \varepsilon_c < \varepsilon_{c,lim} \tag{7}$$

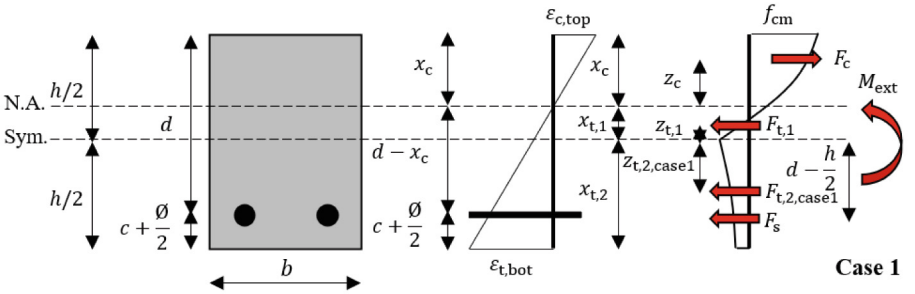

A. Equilibrium relations for case 1

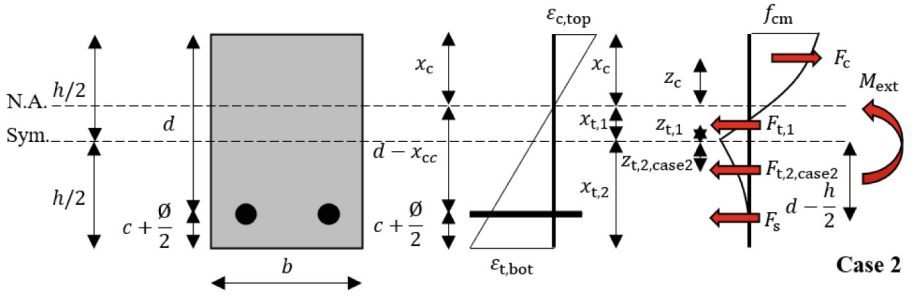

B. Equilibrium relations for case 2

Fig. 1. Strain and stress plots for cases 1 and 2, used to derive equations Eqs. (5) and (6). For an explanation of the various variables and the meaning of cases 1 and 2 is referred to the explanation of Eqs. (7)–(23). N.A. = neutral axis, sym = symmetry line.

With

$$\eta = \varepsilon_c/\varepsilon_{c,1}, k = E_{c,i}/E_{c,1}, \tag{8}$$

where σ_c denotes the concrete compression stress, f_{cm} the average concrete compression strength, ε_c the strain in the concrete element, which varies linearly over the height of the cross-section by the adoption of the assumption that plane sections remain plane during bending, $\varepsilon_{c,1}$ the strain at maximum compressive stress, $\varepsilon_{c,lim}$ the maximum allowable ε_c, $E_{c,i}$ the tangent short-term modulus of elasticity of concrete and $E_{c,1}$ the secant modulus from the origin to the peak of the compression curve. The concrete compression force, F_c, was then computed by integrating σ_c over the height of the compression zone, thus

$$F_c = b \int_0^{x_c} \sigma_c dz, \tag{9}$$

The corresponding centre of gravity z_c of F_c is given by

$$z_c = \left(\int_0^{x_c} z\sigma_c dz\right)/\left(\int_0^{x_c} \sigma_c dz\right). \tag{10}$$

The tensile part of the cross-section $F_{t,1}$, corresponding to $\sigma_t \leq f_{ctm}$, is given by

$$F_{t,1} = x_{t,1} f_{ctm} b/2, \tag{11}$$

where $x_{t,1}$ represents the height of the part of the cross-section related to $F_{t,1}$, and can be calculated by

$$x_{t,1} = \frac{f_{ctm}}{\varepsilon_{c,top} E_c} x_c, \tag{12}$$

where $\varepsilon_{c,top}$ denotes the strain at the top of the concrete element. $x_{t,1}$ was calculated based on the assumed distribution of ε_c over the height of the concrete element, see Fig. 1. For the part related to $\sigma_{ct} > f_{ctm}$, the tension softening curve developed by Hordijk et al. [12–14] was selected, which is presented by

$$\sigma_{ct} = f_{ctm}\left[\left(1 + \left(c_1 \frac{\Delta u_n}{\Delta u_{n,\,ult}}\right)^3\right)\exp\left(-c_2 \frac{\Delta u_n}{\Delta u_{n,\,ult}}\right) - \frac{\Delta u_n}{\Delta u_{n,\,ult}}\left(1 + c_1^3\right)\exp(-c_2)\right], \tag{13}$$

where σ_{ct} indicate the tensile stress, which is a function of the crack width Δu_n according to the tension softening curve. The implementation of the Hordijk curve allowed for a non-linear calculation of σ_{ct}. Linear softening stress-strain relationships also exist but are simplifications of the non-linear ones [6]. The ultimate crack width $\Delta u_{n,\,ult}$ is the crack width Δu_n where the concrete still can transfer σ_{ct}. c_1 and c_2 are coefficients which define the shape of the tension softening curve. Eq. (13) is only valid for $\Delta u_n < \Delta u_{n,ult}$, which is associated to case 1, otherwise σ_{ct} is 0 MPa. If $\Delta u_{n,\,ult}$ in the cross section is reached, then $\sigma_{ct} = 0$ in the parts of a specific crack where $w > \Delta u_{n,ult}$. This is described by case 2. This implies that the distribution of w over the height of the crack is needed. However, in this paper, it was assumed that w is proportional to the strain distribution over the height of the cross-section, allowing that only one point of w needs to be measured. In this paper measurements of w at the most tension face were used; this will be discussed in the results section. If $w \leq \Delta u_{n,\,ult}$, tension softening according to Eq. (13) Was applied; this is called case 1. $\Delta u_{n,ult}$ is calculated by

$$\Delta u_{n,\,ult} = 5.136\, G_f^I / f_{ctm},\ G_f^I = 73 f_{cm}^{0.18}, \tag{14}$$

where G_f^I represents the fracture energy according to fracture mode I and was estimated according to [6]. To convert $\Delta u_{n,\,ult}$ to an ultimate strain $\varepsilon_{n,ult}$, $\Delta u_{n,\,ult}$ was smeared over a crack bandwidth l_{cs} according to [6] $\Delta u_{n,\,ult}$ can then be converted to an ultimate strain by

$$\varepsilon_{n,\,ult} = 5.136 \frac{G_f^I}{f_{ctm}} \frac{1}{l_{cs}},\ l_{cs} = \min\left(s_{r,m}, y\right). \tag{15}$$

In Eq. (15), $s_{r,m}$ denotes the average crack spacing and y the distance from the N.A. to the bottom tension fibre, evaluated based on a cracking analysis in the elastic phase, neglecting the residual tensile strength of the concrete. $F_{t,2,case1}$, representing the force related to the non-linear Hordijk Softening curve based on case 1, was then calculated as

$$F_{t,2,case1} = b \int_0^{x_{t,2,case1}} \sigma_{ct} dz, \tag{16}$$

where the centre of gravity $z_{t,2,case1}$ is described by

$$z_{t,2,case1} = \left(\int_0^{x_{t,2,case1}} z\sigma_{ct}\mathrm{d}z\right)/\left(\int_0^{x_{t,2,case1}} \sigma_{ct}dz\right). \tag{17}$$

Finally, the tensile force in the reinforcement F_s is given by

$$F_s = \frac{A_s E_s \varepsilon_{c,top}(d - x_c)}{x_c}, \tag{18}$$

derived again based on the strain distribution according to Fig. 1. By substituting Eqs. (7)–(18) into Eqs. (5) and (6), the complete model was determined for case 1.

$F_{t,2}$ for case 2, $F_{t,2,case2}$, was obtained using a similar procedure; the ultimate strain is reached in the cross-section, thus

$$F_{t,2,case2} = \frac{x_{t,2}}{\varepsilon_{n,\,ult}} b \int_0^{\varepsilon_{n,\,ult}} \sigma_{ct} d\,\Delta u_n. \tag{19}$$

The height of the cross-section related to the tension softening zone for case 2, $x_{t,2,case2}$, is described by

$$x_{t,2,case2} = \frac{\varepsilon_{n,\,ult} x_c}{\varepsilon_{c,top}} - x_{t,1}, \tag{20}$$

and the centre of gravity is given by

$$z_{t,2,case2} = \frac{x_{t,2,case2}}{\varepsilon_{n,\,ult}}\left(\int_0^{\varepsilon_{n,\,ult}} \Delta u_n \sigma_{ct} d\,\Delta u_n\right)/\left(\int_0^{\varepsilon_{n,\,ult}} \sigma_{ct} d\,\Delta u_n\right). \tag{21}$$

Equations (19) and (21) were expressed in terms of strains instead of stresses by a scaling factor in front of the integral in order to emphasize that the transition between cases 1 and 2 is determined by $\varepsilon_{n,ult}$. Like case 1, for case 2, the strain distribution was entirely determined by substituting Eqs. (7)–(15) and Eqs. (18)-(21) into Eqs. (5) and (6). The derived non-linear Eqs. (5) and (6) were solved numerically for $\varepsilon_{c,top}$ and x_c, making it a semi-analytical method. In order to find physically admissible solutions or to increase the speed of convergence, an initial guess was used. The initial guess was based on Eq. (1) since that equation expresses x_c in closed form, leading to $x_{c,\,init}$. From the found $x_{c,\,init}$, $\varepsilon_{c,\,top,\,init}$ was based on an initial guess for $\varepsilon_{c,top}$. $\varepsilon_{c,\,top,\,init}$ was derived by applying moment equilibrium on the assumptions related to the Schrier method. $\varepsilon_{c,\,top,\,init}$ is given by

$$\varepsilon_{c,\,top,\,init} = \frac{2M_{ext}}{E_c b x_{c,\,init}\left(d - \frac{x_{c,\,init}}{3}\right)}, \tag{22}$$

Finally, from the solved x_c and $\varepsilon_{c,\,top}$ from Eqs. (5) and (6), x_c and $\varepsilon_{c,\,top}$ were back substituted into Eq. (18), from which $\hat{\sigma}_s$ was computed by

$$\hat{\sigma}_s = F_s/A_s. \tag{23}$$

The complete calculation procedure is summarized in Fig. 2.

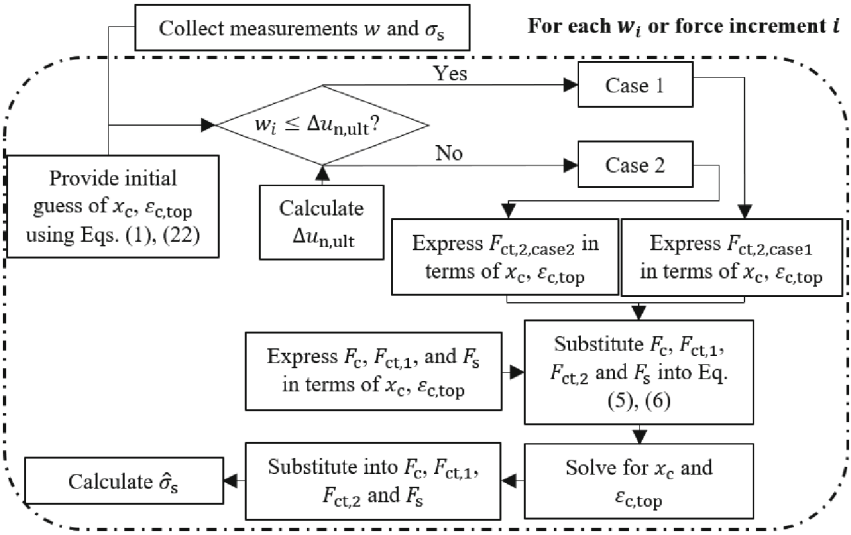

Fig. 2. Workflow for calculating $\hat{\sigma}_s$ of the developed method.

4 Results and Validation

The model was validated based on the experiments of Berrocal et al. [15]. In these experiments, ε_s was measured using DOFs, and w was estimated using digital image correlation (DIC). In this paper, the measured value of ε_s was converted to σ_s by multiplying ε_s with E_s. The experimental program consisted of six beams, tested in a three-point bending test, see Fig. 3. The load at mid-span was applied in a displacement-controlled manner. From the experimental program by [15], beams no. (1) and (2) were selected, which were monotonically loaded, to exclude the effect of load repetitions. The beams had cross-section dimensions of b=100 mm, h=150 mm, and d=120 mm. The reinforcement consisted of two reinforcement bars with a diameter Ø of 10 mm and E_s=200 GPa. The span of the beams was 800 mm. Even though the slenderness $\lambda = L/h$ of the beam is close to 5; still the assumption of plane sections remaining plane was adopted due to the lack of other experiments with larger values of λ. The mean cubic strength $f_{cm,cube}$, following from testing cubes 150x150x150 mm from the concrete batch, was 61 MPa and f_{ctm} was based on a mean splitting tensile strength of 4 MPa. In this paper, based on these provided material properties of [15], the characteristic cylindrical compression strength f_{ck}, which is needed for further validating the developed model, was determined by

$$f_{ck} = 0.8513 f_{cm,\,cube} - 5, f_{cm} = f_{ck} + 8. \tag{24}$$

Eq. (24) Was derived using linear regression applied to the concrete compression properties described in [6]; the regression approach was inspired by Wijte et al. [16]. Applying Eq. (24) And inserting 61 MPa for $f_{cm,\,cube}$ led to a f_{ck} of 46.9 MPa.

Regarding the measurements of [15], the DOFs had a spatial resolution of 0.625mm and a sampling rate of 5 Hz. This is larger than the sampling rate of the applied DIC

system of 0.2 Hz. The spatial resolution of the DOFs was small compared to l_{cs}, thus the measurement of ε_s of the DIC in the vicinity of a crack was very similar to the situation that ε_s would be measured in a crack. This implied that ε_s could be determined accurately, whether the spatial point of the DOF was located in a crack or in the vicinity of that specific crack. The noise value was 10 με (microstrain), corresponding to an estimated noise for σ_s of 2 MPa. The crack pattern was also visualized using DIC, which provided an accuracy of 8.5 μm for the described DIC setup.

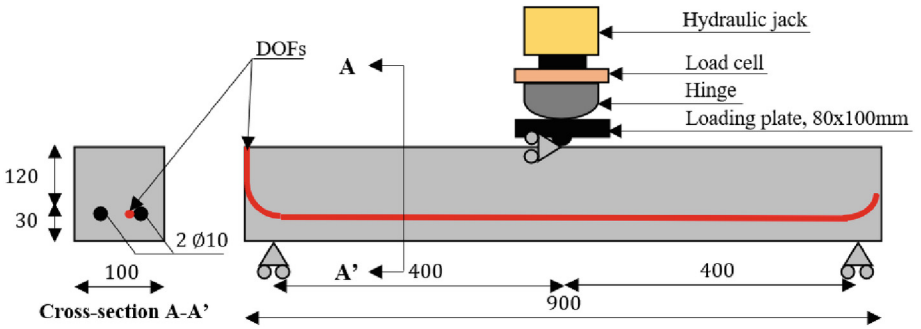

Fig. 3. Experimental setup from [15]

During the experiments of [15], the applied force F_{ext} was measured at the same time intervals as the DIC. However, due to the difference between the sampling rates of the DIC and DOFs and to be able to validate the presented method in this paper with the provided data from [15], linear interpolation was performed on the forcing and time scale of the DIC to compare results from DIC with DOFs.

The estimation of l_{cs} according to Eq. (15) required the computation of $s_{r,m}$ and y. . Since only crack (4) w was estimated by DIC, $s_{r,m}$ was in this paper calculated based on the average of the crack spacing s_r between crack (3) and (4) and the spacing between crack (4) and crack (5), see Fig. 4. w was rather estimated than calculated since DIC was used by [15] to analyze w at the tension face of the beams, which might differ from w located at the reinforcement bars. Nonetheless, due to the limited width of 100 mm, it was assumed that the estimated w is close to the observed w by DIC. This led for beam (1) and (2) to $s_{r,m} = 101$ mm and $s_{r,m} = 86$ mm, respectively. These values were comparable to the distance from the N.A. to the bottom fibre according to Eq. (15), hence for l_{cs} the mean crack spacing was implemented.

For beam (1) and beam (2), 4147 and 2, 4200 measurement points from [15] were selected, respectively. The number of analyses was related to the selected applied forces F resulting from the displacement controlled loading, which resulted in M_{ext} at the location of crack (4). The lower bound of F was selected as the point where for crack (4) a width of 0.05 mm was reached. The choice of 0.05 mm was based on two reasons: 1) it was used as a lower bound F_{low} for the determination of the crack locations in the paper of [15]; 2) a small $w \leq 0.05$ mm cannot be measured by DIC with the same relative accuracy compared to a larger w. The upper bound F_{up} of the applied force was chosen before some NaN values were encountered, close to the end of the measurements. With

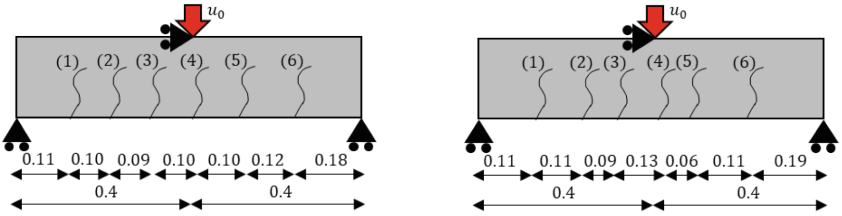

A. Location of the cracks for beam 1. Location of (4) w.r.t. left support: 0.403 m.

B. Location of the cracks for beam 2, Location of (4) w.r.t. left support: 0.439 m.

Fig. 4. Location of cracks, A) beam 1, B) beam 2. The crack number i is denoted as (i). s_r is indicated with black arrows; the distances are indicated in m. u_0 denotes the imposed deformation, which represents the applied load on the concrete element, varying between a lower F_{low} and an upper F_{up} bound.

these starting and ending points of the analyses, almost all available information was considered. See Fig. 5 for the considered moments and the related crack widths, with their corresponding time. The effect of the load due to a self-weight of 0.375 kN/m was neglected since the applied external bending moment M_{ext}, , at the location of crack (4), due to a load of F_{low}, was over 50 times the bending moment due to self-weight. The results showed an approximately linear correlation between M_{ext} and w.

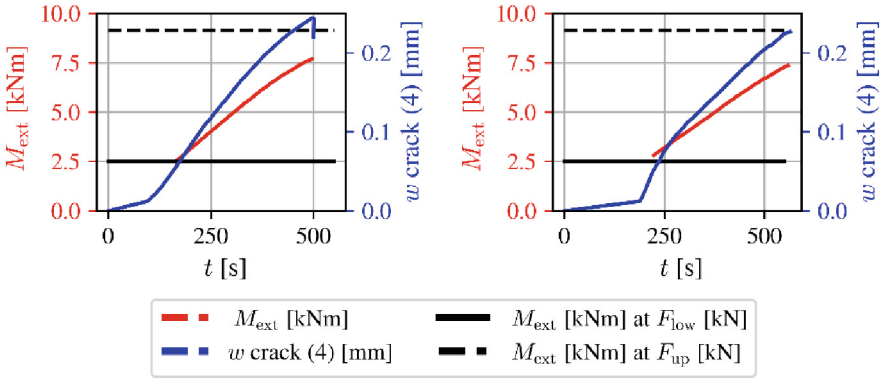

Fig. 5. Loading sequences. Left figure: beam (1). Right figure: beam (2).

In Fig. 6, $\hat{\sigma}_s$ is presented versus the estimated w according to DIC. $\hat{\sigma}_s$ according to the Schrier and Interpolation method are compared with the developed method in this paper, and the computed σ_s according to the measured strains. The figure reveals that all methods in these ranges were approximately describing a linear relation between $\hat{\sigma}_s$ and w. This is reasonable since a single crack is considered; thus, w is then more or less proportional to σ_s. The developed method showed less overestimation of $\hat{\sigma}_s$ with respect to σ_s, calculated based on ε_s measured by the DOFs. The overestimation was still most severe in the early stage of the cracking process, thus when M_{ext} was close to M_{ext} at F_{low}, but provided in these regions still $\approx 30 - 50\%$ less overestimation compared

to the Schrier and Interpolation methods. The reason is that the strains over the height of the cross-section, based on the assumption of the developed method, are relatively small compared to the Schrier method, leading to a smaller value of ε_s. The $\varepsilon_{c,\,top}$ for the developed method compared to the Interpolation method is small; however, the developed method has a larger x_c, leading to a smaller ε_s and thus a smaller $\hat{\sigma}_s$. This is depicted in Fig. 7. Interestingly, the Interpolation method led to minor stresses than the Schrier method. This was reasonable since the first method is computed as an interpolation of M_{ext}/M_R, leading to smaller x_c, consequently a larger z and thus a smaller $\hat{\sigma}_s$. The three methods converge for larger w and thus a larger F_{ext}. Since the tension softening effect decreases for large loads, $\hat{\sigma}_s$ according to the developed method leads to approximately the same value of $\hat{\sigma}_s$ according to the Schier and the Interpolation methods. The described behaviour was generally the same for beams (1) and (2).

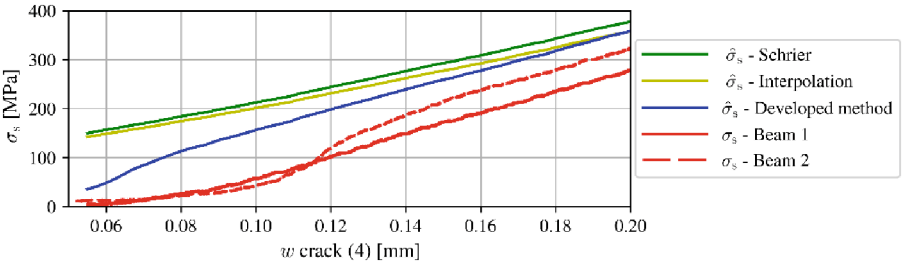

Fig. 6. σ_s vs. estimated crack width w for the Schrier, Interpolation and the developed method for the calculation of $\hat{\sigma}_s$. In red: $\hat{\sigma}_s$ based on the measured values of ε_s according to [15], for beams (1) and (2).

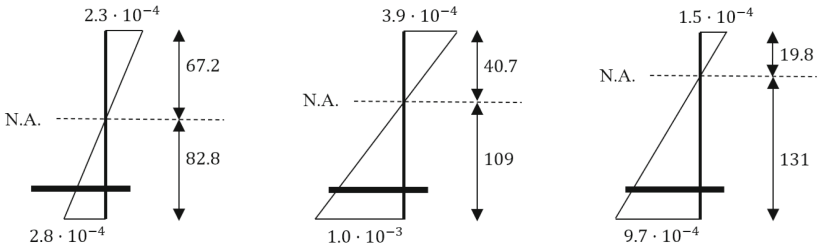

A. Developed method **B.** Schrier method **C.** Interpolation method

Fig. 7. Strain distribution over the height of the cross-section depicted for beam (1), for M_{ext} at F_{low}. The results of beam (2) show similar behaviour and are therefore not depicted.

5 Conclusions and Discussion

This paper discussed the Schrier and Interpolation methods to calculate steel stresses in reinforced concrete elements subjected to bending with a rectangular cross-section and compared them with a method based on more complex constitutive relations for reinforced concrete. It demonstrated that the existing Schrier and Interpolation methods underestimate the steel stress, especially in the initial cracking stage. It also showed that existing methods describe the steel stress relatively accurate at the end of the cracking process. The developed method can estimate the steel stresses during the complete cracking stage with less overestimation and more accuracy. Furthermore, the resulting stresses have the same magnitude as those calculated based on DOFs. However, before the developed method can be applied, it could be simplified and verified based on more experiments tested with DOFs and DICs. More slender beams should be tested in future experiments to satisfy the assumption that plane sections remain plane during bending since that assumption was adopted for the presented semi-analytical method. The results in this paper present a workflow and method for comparing various methods to calculate steel stresses and are not meant for a final comparison since only measurements from two beams were used. This can be done in future research using more measurements from the combined application of DOFS and DICs. The presented method can easily be extended to several cross-sections or more sophisticated reinforcement configurations like multiple reinforcement layers. It can also describe steel stresses more accurately when comparing crack width formulations.

Acknowledgements. The authors thank Rijkswaterstaat Grote Projecten en Onderhoud (GPO) for their financial support and valuable feedback while writing this paper. The support of Carlos G. Berrocal for the provision of data and explanation is much appreciated.

Supporting Files. The source code for the computation is available online: https://github.com/iavdesch.

References

1. Otieno, M., Alexander, M., Beushausen, H.: Corrosion in cracked and uncracked concrete - influence of crack width, concrete quality and crack reopening. Mag. Concr. Res. **62**(6), 393–404 (2010)
2. Scott, A., Alexander, M.: The influence of binder type, cracking and cover on corrosion rates of steel in chloride-contaminated concrete. Mag. Concr. Res. **59**(7), 494–505 (2007)
3. Otieno, M., Beushausen, H., Alexander, M.: Resistivity-based chloride-induced corrosion rate prediction models and hypothetical framework for interpretation of resistivity measurements in cracked RC structures. Mater. Struct. **49**(6), 2349–2366 (2015). https://doi.org/10.1617/s11527-015-0653-z
4. EN 1992–1–1 - Eurocode 2: Design of concrete structures - Part 1–1: General rules and rules for buildings (2011)
5. Allam, S.M., Shoukry, M.S., Rashad, G.E., Hassan, A.S.: Crack width evaluation for flexural RC members. Alex. Eng. J. **51**(3), 211–220 (2012)
6. Model Code 2010. International Federation for Structural Concrete *fib*, Lausanne, Switzerland (2010)

7. van der Schrier, W.: Bouwen in Gewapend Beton, 's-Gravenhage': Argus (1965)
8. Tomislav, K., Ivan, P.: Preliminary dimensioning of reinforced concrete sections. J. Croatian Assoc. Civil Eng. **66**(12), 1125–1140 (2015)
9. Balázs, G., et al.: Design for SLS according to *fib* Model Code 2010. Struct. Concr. **14**(2), 99–123 (2013)
10. Allam, S.M., Shoukry, M.S., Rashad, G.E., Hassan, A.S.: Evaluation of tension stiffening effect on the crack width calculation of flexural RC members. Alex. Eng. J. **52**(2), 163–173 (2013)
11. Lapi, M., Orlando, M., Spinelli, P.: A review of literature and code formulations for cracking in R/C members. Struct. Concr. **19**(5), 1481–1503 (2018)
12. Diana FEA: 21.1.3 Nonlinear Tension Softening (Hordijk et al.), 29 November (2010). https://manuals.dianafea.com/d943/MatLib/node305.html. (Accessed 24 11 2022).
13. Hordijk, D.A.: Local approach to fatigue of concrete. W.D. Meinema b.v., Delft, The Netherlands (1991)
14. Cornelissen, H., Hordijk, D., Reinhardt, H.: Experimental determination of crack softening characteristics of normalweight and lightweight. Heron **31**(2), 45–56 (1986)
15. Berrocal, C.G., Fernandez, I., Rempling, R.: Crack monitoring in reinforced concrete beams by distributed optical fiber sensors. Struct. Infrastruct. Eng. **17**(1), 124–139 (2021)
16. Wijte, S.: Onderzoek constructieve veiligheid breedplaatvloeren in bestaande utiliteitsgebouwen. Adviesbureau ir. J.G. Hageman B.V., Rijswijk (ZH) (2019)